

LINVIDEO: A Post-Training Framework towards $\mathcal{O}(n)$ Attention in Efficient Video Generation

Yushi Huang^{1,3*} Xingtong Ge¹ Ruihao Gong^{2,3†} Chengtao Lv^{3,4*} Jun Zhang^{1†}

¹Hong Kong University of Science and Technology ²Beihang University ³Sensetime Research ⁴Nanyang Technological University

{yhuangin, xingtong.ge}@connect.ust.hk, gongruihao@buaa.edu.cn
chengtao001@e.ntu.edu.sg, eejzhang@ust.hk

Abstract

Video diffusion models (DMs) have enabled high-quality video synthesis, but their computation costs scale quadratically with sequence length due to the nature of self-attention. While linear attention offers a more efficient alternative, fully replacing quadratic attention demands costly pretraining. This is largely because linear attention lacks sufficient expressiveness and struggles with the complex spatiotemporal dynamics inherent to video generation. In this paper, we present LINVIDEO, an efficient data-free post-training framework that replaces a target number of self-attention modules with linear attention while preserving performance. First, we observe a significant disparity in the replaceability of different layers. Instead of manual or heuristic choices, we frame layer selection as a binary classification problem and propose a selective transfer, which automatically and progressively converts layers to linear attention with minimal performance impact. Additionally, to overcome the ineffectiveness and even inefficiency of existing objectives in optimizing this challenge transfer process, we introduce an anytime distribution matching (ADM) objective that aligns the distributions of samples across any timestep along the sampling trajectory. This objective is highly efficient and recovers model performance. Extensive experiments show that LINVIDEO achieves a 1.43–1.71× speedup while preserving generation quality, and the 4-step distilled models further reduce latency by 15.9–20.9× with only a minor drop in visual quality.

1. Introduction

Recently, advances in artificial intelligence-generated content (AIGC) have yielded notable breakthroughs across text [6, 40], image [21, 47], and video synthesis [19, 44]. Progress in video generative models, largely enabled by

the diffusion transformer (DiT) architecture [31], has been particularly striking. State-of-the-art video diffusion models (DMs), including the closed-source OpenAI Sora [30] and Kling [20], as well as the open-source Wan [44] and CogVideoX [50], effectively capture *physical consistency*, *semantic scenes*, and other complex phenomena. Nevertheless, by introducing a temporal dimension relative to image DMs, video DMs greatly increase the sequence length n to be processed (e.g., generating a 10s video often entails $> 50K$ tokens). Consequently, the self-attention operator, whose cost scales quadratically with n in a video DM, becomes a prohibitive bottleneck for deployment.

Prior work has addressed this challenge by designing more efficient attention mechanisms. These methods fall into two categories: (i) attention sparsification [22, 45, 60], which skips redundant dense-attention computations; and (ii) linear attention [3] and its variants [4, 43], which modify computation and architectures to reduce the time and memory complexity from $\mathcal{O}(n^2)$ to $\mathcal{O}(n)$. However, sparsification often cannot reach high sparsity at moderate sequence lengths and, in practice, still retains more than 50% computation of quadratic dense attention. While linear attention offers much lower complexity, replacing *all* quadratic attention layers with linear attention recovers video quality only through time- and resource-intensive pretraining [3, 43]. This arises from (i) the clear representation gap [58] between quadratic and linear attention and (ii) the complexity of spatiotemporal modeling for video generation, both of which make cost-effective post-training impractical and limit the adoption of linear attention. This paper therefore asks: *Can we, via efficient post-training, replace as many quadratic attention layers as possible with linear attention so that effective inference acceleration is achieved without degrading the performance of video DMs?*

To address this challenge, we present LINVIDEO, an efficient *data-free* post-training framework for a pre-trained video DM that selectively replaces a large fraction of $\mathcal{O}(n^2)$ self-attention with $\mathcal{O}(n)$ attention, while preserving output quality. To begin with, we construct training data

*Work done during their internships at SenseTime Research.

†Corresponding authors.

from the pre-trained model’s own inputs and outputs, removing the need for curated high-quality video datasets. Then, we introduce two techniques that (i) choose which attention layers to replace with minimal performance loss and (ii) optimize post-training to recover the original performance, respectively.

Specifically, we find that replacing different layers with linear attention results in significantly varying performance. Guided by this observation, we propose a learning-based *selective transfer* method that progressively and automatically replaces a target number of quadratic attention layers with linear attention, while incurring minimal performance loss. For each layer, we cast the choice as a binary classification problem and use a learnable scalar to produce a classification score in $[0, 1]$ for the two classes (quadratic *vs.* linear). After training, we round the score to pick the type of attention in inference. We also add a constraint loss to steer the total number of selected linear layers toward the target, as well as a regularization term that drives the scores toward 0/1 to reduce rounding error and training noise.

Nevertheless, it is still challenging to optimize video DMs in the above transfer process. Direct output matching on the training set introduces temporal artifacts and weakens generalization. Few-step distillation [51, 52] aligns only final sample distributions and ignores intermediate timesteps, causing notable drops in our setting. Furthermore, it needs an auxiliary diffusion model to estimate the generator’s score function [37]. Based on these findings, we propose an *anytime distribution matching* (ADM) objective that aligns sample distributions at any timestep along the sampling trajectory, and we estimate the score function using the current model itself. This objective effectively preserves model performance while enabling efficient training.

To summarize, our contributions are as follows:

- We introduce, to our knowledge, the *first* efficient *data-free* post-training framework, LINVIDEO, that replaces quadratic attention with linear attention in a pre-trained video DM, enabling efficient video generation without compromising performance.
- We propose *selective transfer*, which automatically and smoothly replaces a target number of quadratic attention with linear attention, minimizing performance drop.
- We present an *anytime distribution matching* (ADM) objective that effectively and efficiently aligns the distributions of samples from the trained model and the original DM at any timestep.
- Extensive experiments show that our method achieves a **1.43–1.71 \times** latency speedup and outperforms prior post-training methods on VBench. Moreover, we are the *first* to apply few-step distillation to a linear-attention video DM. Remarkably, the 4-step models attain a **15.9–20.9 \times** speedup.

2. Related Work

Video DMs. Video generation has emerged as a rapidly growing area in generative AI, with most approaches built on the denoising diffusion paradigm. A major breakthrough—enabling high compression rates and long-form generation—arrived with Sora [30], which introduced a temporal variational auto-encoder (VAE) that compresses temporal as well as spatial dimensions and scaled up the diffusion transformer (DiT) [31] architecture for video generation. Subsequent efforts [9, 12, 19, 34, 44, 50] have further advanced this modern design space. For example, CogVideoX [50] introduced expert-adaptive LayerNorm to improve text–video fusion, while Wan 2.2 [44] incorporated a sparse mixture-of-expert (MoE) [35] that routes diffusion steps to specialized experts. Alongside methodological progress, recent large-scale deployments underscore the transformative potential of video generation. Systems such as Kling [20] and Seaweed [34] demonstrate substantial practical impact across creative and industrial applications. Taken together, these advances establish video generation as one of the most dynamic and competitive frontiers within the generative AI community.

Efficient attention for video DMs. There have been lots of studies [7, 45] on video diffusion models (DMs) aiming to accelerate inference by sparsifying computationally expensive dense 3D attention. These methods fall into two categories: *static* and *dynamic*. *Static* methods [22, 38, 59, 60] predefine a sparsity pattern offline by identifying critical tokens. However, these methods fail to capture the dynamics of sparsity patterns during inference, leading to suboptimal performance. *Dynamic* methods [39, 45, 48, 57, 61] adapt the sparsity pattern at inference time based on input content. Thus, they need to select critical tokens through an additional identification step. Other approaches [24, 63] combine sparsification with quantization to further reduce latency and memory usage.

Meanwhile, linear attention [8] and its alternatives (*e.g.*, state space models [13]) for video generation have also gained attention. Most of these works [3, 4, 10, 16, 43] focus on a costly pretraining manner initialized from a given image generative model [46]. Among them, Matten [10] and LinGen [43] adopt Mamba [13] to capture global information. SANA-Video [3] involves auto-regressive training [2] with block-wise causal linear attention. To the contrary, we explore applying linear attention to advanced pre-trained video DMs [44]. One concurrent work, SLA [56], proposes intra-layer mixed attention (*e.g.*, quadratic and linear attention) in a post-training manner. Instead, we concentrate on inter-layer mixed attention (*i.e.*, replacing partial layers with linear attention). Moreover, we believe our data-free finetuning with the proposed strategy can be combined with SLA for more efficient and high-performing linearization for video DMs.

3. Preliminaries

Video diffusion modeling. The video DM [15, 66] extends image DMs [23, 36] into the temporal domain by learning dynamic inter-frame dependencies. Let $\mathbf{x}_0 \in \mathbb{R}^{f \times h \times w \times c}$ be a latent video variable, where f denotes the count of video frames, each of size $h \times w$ and with c channels. DMs are trained to denoise samples generated by adding random Gaussian noise $\epsilon \sim \mathcal{N}(\mathbf{0}, \mathbf{I})$ to \mathbf{x}_0 :

$$\mathbf{x}_t = \alpha_t \mathbf{x}_0 + \sigma_t \epsilon, \quad (1)$$

where $\alpha_t \geq 0$, $\sigma_t > 0$ are specified noise schedules such that $\frac{\alpha_t}{\sigma_t}$ is monotonically decreasing w.r.t. timestep t and a larger t indicates greater noise. With noise prediction parameterization [14] and discrete-time schedules (i.e., $t \in [1, \dots, T]$ and typically $T = 1000$), the training objective for a neural network ϵ_θ parameterized by θ can be formulated as follows:

$$\mathbb{E}_{\mathbf{x}_0, \epsilon, \mathcal{C}, t} [w(t) \|\epsilon - \epsilon_\theta(\mathbf{x}_t, \mathcal{C}, t)\|_F^2], \quad (2)$$

where \mathcal{C} represents conditional guidance, such as texts or images, $w(t)$ is a weighting function, and $\|\cdot\|_F$ denotes the Frobenius norm. Advanced video DMs [19, 44] are *flow matching models* [25]. They employ velocity prediction parameterization [33] and continuous-time coefficients. In *rectified flow models* [42], the standard choice is $\alpha_t = 1 - t$, $\sigma_t = t$ for $t \in [0, 1]$, which is the setting adopted in this work. The conditional probability path or the velocity is given by $\mathbf{v}_t = \frac{d\alpha_t}{dt} \mathbf{x}_0 + \frac{d\sigma_t}{dt} \epsilon$, and the corresponding training objective is:

$$\mathbb{E}_{\mathbf{x}_0, t, \mathcal{C}, \epsilon} [w(t) \|\mathbf{v}_t - \mathbf{v}_\theta(\mathbf{x}_t, \mathcal{C}, t)\|_F^2], \quad (3)$$

where \mathbf{v}_θ is a neural network parameterized by θ . The sampling procedure of these models begins at $t = 1$ with $\mathbf{x}_1 \sim \mathcal{N}(\mathbf{0}, \mathbf{I})$ and stops at $t = 0$, solving the *Probability-Flow Ordinary Differential Equation* (PF-ODE) by $d\mathbf{x}_t = \mathbf{v}_\theta(\mathbf{x}_t, \mathcal{C}, t) dt$.

After obtaining \mathbf{x}_0 through iterative sampling, the raw video is obtained by decoding the variable via a video variational auto-encoder (VAE) [44].

Attention computation. Given input $\mathbf{x} \in \mathbb{R}^{n \times d}$ (where n denotes the sequence length and d signifies the feature dimension), attention is written as:

$$\mathbf{o}_i = \sum_{j=1}^n \frac{\text{sim}(\mathbf{q}_i, \mathbf{k}_j)}{\sum_{j=1}^n \text{sim}(\mathbf{q}_i, \mathbf{k}_j)} \mathbf{v}_j, \quad (4)$$

where $\mathbf{q} = \mathbf{x}\mathbf{W}_q$, $\mathbf{k} = \mathbf{x}\mathbf{W}_k$, $\mathbf{v} = \mathbf{x}\mathbf{W}_v$ and $\mathbf{W}_q/\mathbf{W}_k/\mathbf{W}_v \in \mathbb{R}^{d \times d}$ are learnable projection matrices. i/j are row indices for their corresponding matrices and $\text{sim}(\cdot, \cdot)$ indicates the similarity function. When employing $\text{sim}(\mathbf{q}, \mathbf{k}) = \exp(\frac{\mathbf{q}\mathbf{k}^\top}{\sqrt{d}})$, Eq. (4) represents standard *softmax attention* [41]. In this way, the attention map computes

the similarity between all query-key pairs, which causes the computational complexity to be $\mathcal{O}(n^2)$.

In contrast, *linear attention* [18] adopts a carefully designed kernel $k(x, y) = \langle \phi(x), \phi(y) \rangle$ as the approximation of the original function (i.e., $\text{sim}(\mathbf{q}, \mathbf{k}) = \phi(\mathbf{q})\phi(\mathbf{k})^\top$). In this case, we can leverage the associative property of matrix multiplication to reduce the computational complexity from $\mathcal{O}(n^2)$ to $\mathcal{O}(n)$ without changing functionality:

$$\mathbf{o}_i = \sum_{j=1}^n \frac{\phi(\mathbf{q}_i)\phi(\mathbf{k}_j)^\top}{\sum_{j=1}^n \phi(\mathbf{q}_i)\phi(\mathbf{k}_j)^\top} \mathbf{v}_j = \frac{\phi(\mathbf{q}_i) \left(\sum_{j=1}^n \phi(\mathbf{k}_j)^\top \mathbf{v}_j \right)}{\phi(\mathbf{q}_i) \left(\sum_{j=1}^n \phi(\mathbf{k}_j)^\top \right)}. \quad (5)$$

In this work, we directly employ the effective kernel design from *Hedgehog* [58], which is formulated as:

$$\phi(\mathbf{q}) = \text{softmax}(\mathbf{q}\widetilde{\mathbf{W}}_q) \oplus \text{softmax}(-\mathbf{q}\widetilde{\mathbf{W}}_q), \quad (6)$$

where $\widetilde{\mathbf{W}}_q \in \mathbb{R}^{d \times \frac{d}{2}}$ is a learnable matrix. Both \oplus (concat) and $\text{softmax}(\cdot)$ apply to the feature dimension. The same function applies to \mathbf{k} with another learnable matrix $\widetilde{\mathbf{W}}_k \in \mathbb{R}^{d \times \frac{d}{2}}$.

4. LINVIDEO

In this work, we propose LINVIDEO (see Fig. 1), a post-training framework that selectively replaces softmax attention with linear attention for a pre-trained video DM.

Preparation for data-free post-training. Video diffusion models [30, 44, 50] demand large, diverse datasets, yet access is often limited by scale, privacy, and copyright. To this end, we adopt a *data-free fine-tuning* approach in this work, which transfers the original model’s (i.e., \mathbf{u}_θ) prediction ability to its linear attention version without requiring the original dataset. Specifically, we first randomly sample a large amount of initial noise $\mathbf{x}_1 \sim \mathcal{N}(\mathbf{0}, \mathbf{I})$, and fetch all the input and output pairs of \mathbf{u}_θ in the sampling trajectory (start from \mathbf{x}_1) (i.e., $(\mathbf{x}_t, \mathbf{u}_t)$ for $t \in [0, 1]$) as our training dataset and targets. During fine-tuning, a naive objective can be defined as:

$$\mathcal{L}_{\text{mse}} = \|\mathbf{u}_t - \hat{\mathbf{u}}_\theta(\mathbf{x}_t, t)\|_F^2, \quad (7)$$

where $\hat{\mathbf{u}}_\theta$ is our video DM with linear attention. However, due to the significant representation capability gap [18, 58] between the softmax attention and linear attention, it is challenging to preserve the complex temporal and spatial modeling capabilities of video DMs when (i) directly replacing *all* quadratic attention layers with linear attention modules and (ii) employing naive *data-free fine-tuning*.

In light of this, we propose two novel techniques, *i.e.*, *selective transfer* (Sec. 4.1) and *anytime distribution matching* (Sec. 4.2) to replace maximum softmax attention layers

¹We omit the conditions for simplicity.

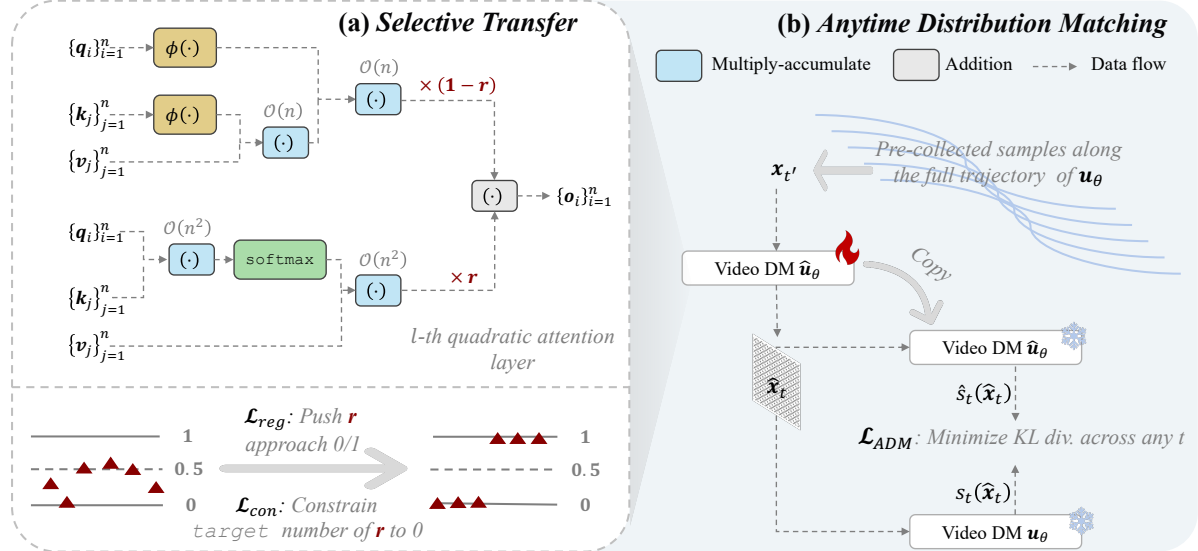


Figure 1. Overview of the proposed efficient *data-free* post-training framework, LINVIDEO. (a) This framework first applies *selective transfer* (Sec. 4.1), which assigns each layer a learnable score r and progressively, automatically replaces quadratic attention with linear attention while minimizing the resulting performance drop. This process also combines with \mathcal{L}_{con} (i.e., Eq. (9)) and \mathcal{L}_{reg} (i.e., Eq. (10)) to ensure a given target number of layers replaced by linear attention and mitigate the fluctuation (around 0.5) of r to improve training, respectively. (b) Moreover, LINVIDEO integrates an *anytime distribution matching* objective (Sec. 4.2), which aims to match the sample distributions between $\hat{\mathbf{u}}_\theta$ and \mathbf{u}_θ across any timestep in the sampling trajectory. This significantly recovers performance and enables high efficiency compared with previous objectives in our scenarios.

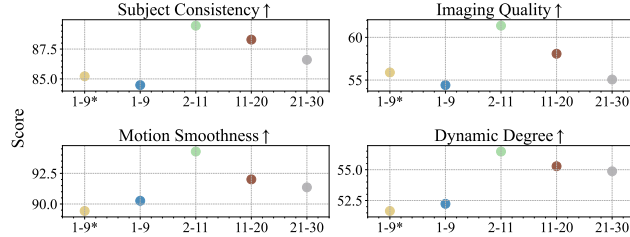


Figure 2. Performance on 4 VBench [17] dimensions for partial linearized (10 adjacent layers for each dot) Wan 1.3B [44] after 2K-step fine-tuning. The index range of the layers replaced with linear attention is indicated in the tick label of the x-axis. “*” denotes models further fine-tuned for 3K additional steps.

with linear attention while preserving the video DM’s exceptional performance. The training overview is presented in Sec. 4.3.

4.1. Selective Transfer for Effective Linearization

In this subsection, we explore how to effectively select layers for linear attention replacement.

Layer selection matters. As described before, we consider replacing partial layers in this work, and we first find that the choice of which layers to replace in a pre-trained video DM can lead to significant performance disparities after fine-tuning. As shown in Fig. 2, this disparity follows two main patterns:

(i) Models with linearized shallow layers recover accuracy more easily than models with linearized deep layers. For instance, applying linear attention from the 2-nd to the 11-th

layer achieves improvements of +2.86 and +6.31 in Subject Consistency and Image Quality, respectively, compared to applying it from the 21-th to the 30-th layer. This may be because errors introduced by shallow layers can be better compensated by the optimization of subsequent layers.

(ii) However, including certain layers, such as the first layer (i.e., blue dots), results in significant performance drops when replaced. These declines can not be mitigated after extended fine-tuning (i.e., yellow dots).

Selective transfer from $\mathcal{O}(n^2)$ to $\mathcal{O}(n)$. Based on the above investigation, we propose *selective transfer* to select partial quadratic attention layers with linear attention replacement. This approach automatically determines which layers to replace. It also enables a progressive and smooth transition from the original softmax attention to linear attention. Specifically, inspired by the binary classification problem, we consider each type of attention (for each layer) as an individual class, opposite to the other. Then, we employ a mixed-attention computation as:

$$\mathbf{o}_i = r \sum_{j=1}^n \frac{\exp(\frac{\mathbf{q}_i \mathbf{k}_j^\top}{d})}{\sum_{j=1}^n \exp(\frac{\mathbf{q}_i \mathbf{k}_j^\top}{d})} \mathbf{v}_j + (1-r) \frac{\phi(\mathbf{q}_i) (\sum_{j=1}^n \phi(\mathbf{k}_j)^\top \mathbf{v}_j)}{\phi(\mathbf{q}_i) (\sum_{j=1}^n \phi(\mathbf{k}_j)^\top)}, \quad (8)$$

where $\phi(\cdot)$ follows Eq. (6) and r is an introduced learnable parameter². In Eq. (8), r and $1-r$ represent the clas-

²In detail, each r is clipped into $[0, 1]$ before computing.

sification score for each class (*i.e.*, quadratic and linear attention, respectively). We initialize $[r^{(1)}, \dots, r^{(N)}] = \mathbf{I} \in \mathbb{R}^{1 \times N}$ to stabilize the training, where N denotes the maximum index of the attention layers. After training, if the classification score for a class is greater than 0.5, the corresponding class is selected for inference. This means we preserve the quadratic attention and remove the linear attention branch when $\lceil r \rceil = 1$, and *vice versa*.

Here, we propose a constraint loss to enforce the video DM with `target` (given before training) layers being replaced with linear attention:

$$\mathcal{L}_{\text{con}} = \left(\sum_{l=1}^N \lceil r^{(l)} \rceil - \text{target} \right)^2. \quad (9)$$

To ensure the differentiability, we employ a straight-through estimator (STE) [1] to r as $\frac{\partial \lceil r \rceil}{\partial r} = 1$.

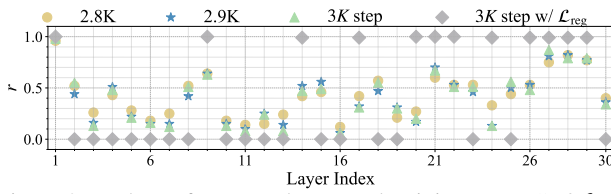


Figure 3. Values of r across layers and training steps. “w/ \mathcal{L}_{reg} ” denotes we employ Eq. (10) for training, otherwise only Eq. (9) is applied to guide the training of r .

Moreover, to force r to approach 0/1 during training, inspired by model quantization [28], we further apply a regularization:

$$\mathcal{L}_{\text{reg}} = \sum_{i=1}^N (1 - |2r^{(i)} - 1|^\alpha), \quad (10)$$

where we annealing decay the parameter α from large to small. This encourages r to move more adaptively at the initial phase to improve the training loss, but forces it to 0/1 in the later phase (see this effect in the Appendix). This regularization helps mitigate the significant performance degradation caused by $\lceil \cdot \rceil$. As demonstrated in Fig. 3, without \mathcal{L}_{reg} , a large number of r values fluctuate around the 0.5 boundary at the end of training. As both attentions in Eq. (8) occupy a non-negligible proportion (*i.e.*, $r \approx 0.5$), directly removing one of them by rounding r for inference can result in significant accuracy drops (as shown in Sec. 5.3). Moreover, the fluctuation of r introduces training noise, which could also disrupt the learning process.

4.2. Match the Distribution across Any Timestep

Our *selective transfer* determines how to select layers for linear attention replacement. In this subsection, we study how to optimize this process.

Objective analysis. The naive optimization objective (*i.e.*, Eq. (7)) leads to temporal artifacts (*e.g.*, flicker and jitter),

as demonstrated in the Appendix, likely because it does not preserve the model’s original joint distribution over frames. This objective also harms generalization by enforcing exact latent alignment on the training set [52]. Prior few-step distillation works [11, 51, 53, 54] address above problems using *distribution matching*, which seeks to align p_g ³ with p_0 ⁴ by minimizing their Kullback–Leibler (KL) divergence during training. However, directly applying this objective in our work faces two key challenges:

(i) *Distribution matching* in few-step distillation only matches p_g against p_0 , discarding distribution p_t ⁵ across timesteps. This leads to considerable performance degradation in our scenario, as demonstrated in Sec. 5.3.

(ii) An additional multi-step DM must be trained to approximate the score [37] determined by p_g , which is required to compute the gradient of the KL divergence between p_g and p_0 . This necessity arises because the few-step generator learns only the naive mapping: $p_T \mapsto p_0$, while its score field remains intractable [51, 52]. Even worse, the additional multi-step DM typically incurs 5–10× generator’s training cost, rendering the approach inefficient.

Anytime distribution matching (ADM). To this end, we propose an *anytime distribution matching* (ADM) method to address challenge (i). Instead of just matching the final data distributions ($t = 0$), the core idea is to match the distributions across any timestep $t \in [0, 1]$ along the entire sampling trajectory. This objective encourages the linearized DM to produce samples whose distribution at every t matches that of the original DM. Specifically, let q_t denote the distributions of $\hat{\mathbf{x}}_t$ ⁶, respectively. For any given t , we minimize the KL divergence between q_t and p_t :

$$\begin{aligned} \mathcal{L}_{\text{ADM}} &= \mathbb{E}_{\hat{\mathbf{x}}_t \sim q_t} \left[\log \frac{q_t(\hat{\mathbf{x}}_t)}{p_t(\hat{\mathbf{x}}_t)} \right] \\ &= \mathbb{E}_{\hat{\mathbf{x}}_t \sim q_t} \left[-(\log p_t(\hat{\mathbf{x}}_t) - \log q_t(\hat{\mathbf{x}}_t)) \right]. \end{aligned} \quad (11)$$

Here, $\hat{\mathbf{x}}_t = (t - t') \hat{\mathbf{u}}_\theta(\mathbf{x}_{t'}, t') + \mathbf{x}_{t'}$ ⁷, where t and t' are adjacent timesteps on the sampling trajectory, and $\mathbf{x}_{t'}$ is collected sample from the original DM in preparation. The gradient of Eq. (11) with respect to the parameters θ of $\hat{\mathbf{u}}_\theta$ can be written as:

$$\frac{\partial \mathcal{L}_{\text{ADM}}}{\partial \theta} = \mathbb{E}_{\hat{\mathbf{x}}_t \sim q_t} \left[-(s_t(\hat{\mathbf{x}}_t) - \hat{s}_t(\hat{\mathbf{x}}_t)) \frac{\partial \hat{\mathbf{x}}_t}{\partial \hat{\mathbf{u}}_\theta} \frac{\partial \hat{\mathbf{u}}_\theta}{\partial \theta} \right], \quad (12)$$

where $s_t(\hat{\mathbf{x}}_t) = \nabla_{\hat{\mathbf{x}}_t} \log p_t(\hat{\mathbf{x}}_t)$, $\hat{s}_t(\hat{\mathbf{x}}_t) = \nabla_{\hat{\mathbf{x}}_t} \log q_t(\hat{\mathbf{x}}_t)$ are the score functions of p_t and q_t , respectively. In

³The distribution of outputs \mathbf{x}_g , which is generated by a few-step generator.

⁴The distribution for the final sample \mathbf{x}_0 , which is generated by the original DM.

⁵ p_t is the distribution of \mathbf{x}_t , which is the sample generated by the original DM at t .

⁶Samples generated by the linearized DM.

⁷We employ the Euler solver for simplicity.

Table 1. Performance comparison with relevant baselines on 8 dimensions of VBench [17]. “+DMD2” denotes our 4-step distilled LINVIDEO model. We highlight the best score and the second score in **bold** and underlined formats, respectively.

Method	Latency (s)↓ Speedup↑		Imaging Quality↑ Aesthetic Quality↑ Motion Smoothness↑ Dynamic Degree↑ Background Consistency↑ Subject Consistency↑ Scene Consistency↑ Overall Consistency↑							
	Wan 1.3B (CFG = 5.0, 480p, fps = 16)									
FlashAttention2 [5]	97.32	1.00×	66.25	59.49	98.42	59.72	96.57	95.28	39.14	26.18
DFA [55]	88.95	1.09×	65.41	58.35	<u>98.11</u>	58.47	95.82	94.31	38.43	26.08
XAttn [48]	83.51	1.17×	65.32	58.51	97.42	59.02	95.43	93.65	38.14	26.22
SVG [45]	74.52	1.31×	65.78	59.16	97.32	58.87	95.79	93.94	38.54	25.87
SVG2 [49]	84.91	1.15×	<u>66.03</u>	<u>59.31</u>	98.07	59.44	<u>96.61</u>	<u>94.95</u>	<u>39.14</u>	<u>26.48</u>
LINVIDEO	68.26	<u>1.43×</u>	66.07	59.41	98.19	<u>59.67</u>	96.72	95.12	39.18	26.52
LINVIDEO + DMD2 [51]	6.110	<u>15.9×</u>	65.62	57.74	97.32	61.26	95.47	93.74	38.78	25.94
Wan 14B (CFG = 5.0, 720p, fps = 16)										
FlashAttention2 [5]	1931	1.00×	67.89	61.54	97.32	70.56	96.31	94.08	33.91	26.17
DFA [55]	1382	1.40×	65.93	60.13	96.87	69.34	95.37	93.26	33.14	26.12
XAttn [48]	1279	1.51×	65.47	60.36	96.28	69.25	95.24	92.97	33.22	<u>26.14</u>
SVG [45]	1203	1.61×	66.09	60.86	96.91	69.46	95.35	93.18	33.46	26.07
SVG2 [49]	1364	1.42×	<u>66.25</u>	<u>61.08</u>	<u>97.12</u>	69.43	<u>95.51</u>	<u>93.39</u>	<u>33.52</u>	26.14
LINVIDEO	<u>1127</u>	<u>1.71×</u>	66.47	61.36	97.24	69.82	96.34	93.68	33.72	26.16
LINVIDEO + DMD2 [51]	92.56	<u>20.9×</u>	65.74	59.68	96.32	<u>69.74</u>	95.38	92.88	33.18	26.09

Eq. (12), s_t pulls \hat{x}_t toward the modes of p_t , whereas $-\hat{s}_t$ pushes \hat{x}_t away from those of q_t .

Under the *rectified-flow* modeling, we estimate s_t with u_θ following Ma *et al.* [27]. For \hat{s}_t , we use the model currently being trained— \hat{u}_θ —which, as a multi-step DM, can estimate its own score function at \hat{x}_t [37]. This property addresses challenge (ii) and substantially improves training efficiency and model performance (see Sec. 5.3). Therefore, the score difference admits the following form (see Appendix for a detailed derivation):

$$s_t(\hat{x}_t) - \hat{s}_t(\hat{x}_t) = -\frac{1-t}{t} (u_\theta(\hat{x}_t) - \hat{u}_\theta(\hat{x}_t)). \quad (13)$$

4.3. Training Overview

In summary, we first collect data pairs from the original video DM. Then we apply learnable parameters $[r^{(1)}, \dots, r^{(N)}]$ with mixed attention (*i.e.*, Eq. (8)) to the model. For training, we adopt the following training loss:

$$\mathcal{L}_{\text{total}} = \mathcal{L}_{\text{ADM}} + \lambda (\mathcal{L}_{\text{con}} + \mathcal{L}_{\text{reg}}), \quad (14)$$

where λ is a hyper-parameter. During training, \hat{u}_θ progressively transfers from a pre-trained multi-step video DM to a high-efficiency video DM with target softmax attention layers replaced with linear attention (*i.e.*, r from 1 to 0).

Moreover, to further enhance inference efficiency, we provide an option to apply a few-step distillation [51] after the above process. To be noted, directly distilling the original DM into a few-step generator with linear attention incurs catastrophic performance drops (see Appendix).

5. Experiments

5.1. Experimental Details

Implementation. We implement LINVIDEO with 50-step Wan 1.3B and Wan 14B models [44], both *rectified flow* text-to-video models that can generate 5s videos at 16 FPS with a resolution of 832×480 (*former*) and 720×1280 (*latter*). Specifically, we first collect 50K inputs and outputs pairs from the model as the training dataset. Then, we set target (see Eq. (9)) to 16 for Wan 1.3B and 22 for Wan 14B, which means we replace $\frac{16}{30}$ or $\frac{22}{40}$ of quadratic attention layers with linear attention. For training, the AdamW [26] optimizer is utilized with a weight decay of 10^{-4} . We employ a cosine annealing schedule to adjust the learning rate over training. Additionally, we train the models for 3K steps on $8 \times$ H100 GPUs for Wan 1.3B and $32 \times$ H100 GPUs for Wan 14B. For our 4-step distilled model, we employ DMD2 [51] and train the model for an additional 2K steps. Latency in this work is tested on a single H100 GPU. More implementation details are in the Appendix.

Evaluation. We select 8 dimensions in VBench [17] with unaugmented prompts to comprehensively evaluate the performance following previous studies [32, 62]. Moreover, we additionally report the results on VBench-2.0 [65] with augmented prompts to measure the adherence of videos to *physical laws, commonsense reasoning, etc.*

Baselines. We compare LINVIDEO with sparse-attention baselines, including the static methods Sparse VideoGen (SVG) [45], Sparse VideoGen 2 (SVG2) [49], and DiTFastAttn (DFA) [55], and the dynamic method XAttention [48]. For latency, we include only the fast attention implementations of these methods to ensure a fair comparison, exclud-

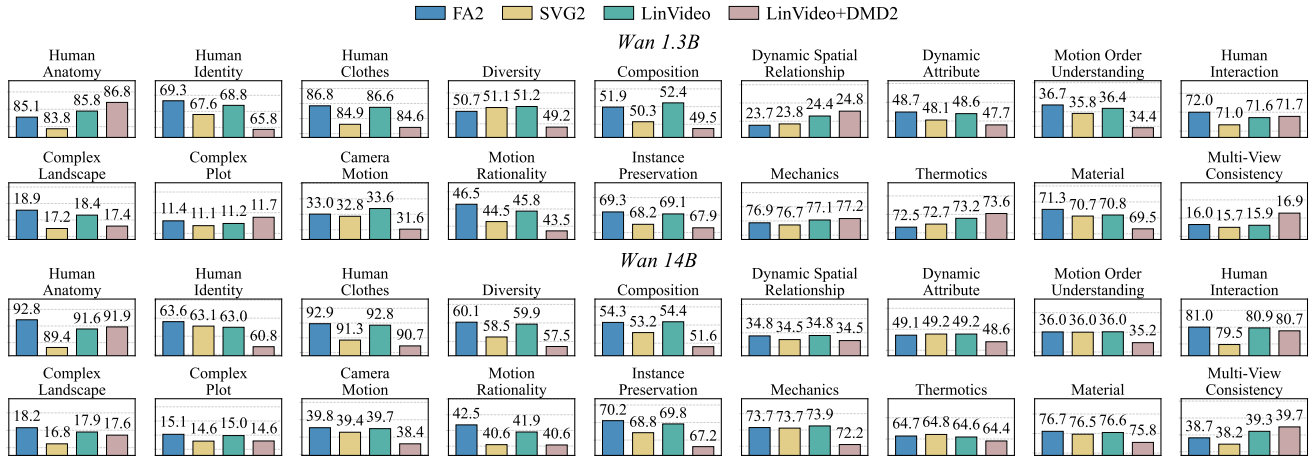


Figure 4. Performance comparison with baselines on VBench-2.0 [65]. For Wan 1.3B, the total scores are 56.74 (FA2), 55.81 (SVG2), 56.74 (LINVIDEO), and 55.51 (LINVIDEO+DMD2); for Wan 14B, the total scores are 59.85 (FA2), 58.74 (SVG2), 59.62 (LINVIDEO), and 58.22 (LINVIDEO+DMD2). FA2 denotes FlashAttention2 [5].



Figure 5. Visual results at 480p across Wan 1.3B [44] (Upper), 1.3B LINVIDEO (Middle), and 1.3B LINVIDEO+ 4-step DMD2 [51] (Lower). Prompt: “A wide pink flower field under a stormy twilight sky with a faint magical glow. Buds burst into luminous blossoms that spread in waves across the meadow. Above, massive black storm clouds roll hard and fast, with layered billows, shelf-cloud structure, and clear turbulence; inner lightning pulses for drama, no ground strikes. A few bioluminescent motes drift between flowers; faint aurora-like ribbons sit behind the storm.”

ing auxiliary designs like the RMSNorm kernel in SVG. To be noted, we also exclude methods that require substantially more training resources [59] compared with LINVIDEO or support only specific video shapes [22]. Moreover, we do not compare our work with SLA [56], since its speedup relies on a specific CUDA kernel implementation that only supports the RTX 5090 GPU.

5.2. Main Results

We compare our method with baselines and benchmark end-to-end latency across baselines using a batch size of 1 with 50 denoising steps in Tab. 1. LINVIDEO consistently far outperforms all sparse-attention baselines and surpasses dense attention (FlashAttention2) on certain metrics, such as Overall Consistency and Scene Consistency. Moreover, our method achieves an average speedup of 1.43-1.71 \times compared with 1.31-1.61 \times for SVG [45]. It is also worth

noting that for LINVIDEO, we do not employ any specialized kernel implementation, which, as a future direction, would allow our method to achieve an enhanced speedup ratio. Notably, when combined with DMD2 [51], 1.3B LINVIDEO yields only a $\sim 1\%$ performance drop while achieving a 15.92 \times end-to-end speedup. Besides, our current design uses only dense linear attention or retains dense quadratic attention. This is orthogonal to sparse-attention methods. Thus, future work could integrate efficient sparse modules into our proposed LINVIDEO to further improve efficiency and performance.

Additionally, we also employ more challenging VBench-2.0 [65] to evaluate performance. We compare our LINVIDEO with the best-performing method SVG2 (see Tab. 1) and the lossless baseline FlashAttention2. As shown in Fig. 4, our method for Wan 1.3B can achieve the same total score as FA2 and a much higher total score than SVG2.

Moreover, our 4-step distilled 1.3B model incurs less than 3% performance drops with higher scores on specific metrics like Human Identity and Multi-View Consistency compared with FA2.

For qualitative results, we present a visualization in Fig. 5, which demonstrates that our method achieves exceptionally high visual quality, even after 4-step distillation. More visual results can be found in the Appendix

5.3. Ablation Studies

We employ 1.3B LINVIDEO for ablation studies. 5 dimensions of VBench are employed to evaluate performance. Unless specified, the settings are the same as those in Sec. 5.

Table 2. Ablation results across different values of `target` (“`tar`”). We employ `target` = 16 in 1.3B LINVIDEO.

<code>tar</code>	Latency ↓	Imaging ↑ Quality	Aesthetic ↑ Quality	Motion ↑ Smoothness	Dynamic ↑ Degree	Overall ↑ Consistency
10	78.14	66.32	59.18	98.68	60.06	26.35
12	74.81	66.36	59.14	98.57	59.73	26.65
14	71.48	66.17	58.88	98.34	59.67	26.29
16	68.26	66.07	59.41	98.19	59.67	26.52
18	65.00	65.84	58.32	97.78	58.63	26.08
20	61.68	64.38	57.02	95.49	57.12	23.30

Choice of `target`. We investigate the effect of different `target` values on the video quality. As shown in Tab. 2, our results reveal that a larger `target` leads to greater acceleration but at the cost of performance degradation, and *vice versa*. Specifically, we find that performance degrades slowly as `target` increases, remaining stable until `tar` = 18, after which we observe a non-negligible drop.

Table 3. Ablation results of *selective transfer*. For LINVIDEO, $\lambda = 0.01$. “*Manual*” denotes we manually assign the same quadratic attention layers as LINVIDEO to linear attention, and “*Heuristic*” signifies we employ a grid search method (details can be found in the Appendix) to determine the indices of quadratic attention layers to be replaced. Both methods employ \mathcal{L}_{ADM} as their training loss after attention replacement. We provide ablations for α of \mathcal{L}_{reg} in the Appendix.

Method	Imaging ↑ Quality	Aesthetic ↑ Quality	Motion ↑ Smoothness	Dynamic ↑ Degree	Overall ↑ Consistency
LINVIDEO	66.07	59.41	98.19	59.67	26.52
<i>Manual</i>	62.97	57.21	92.25	52.87	20.08
<i>Heuristic</i>	60.74	54.13	90.36	50.61	18.94
$\lambda = 0.1$	66.21	59.17	97.94	59.31	26.16
$\lambda = 0.001$	65.98	58.96	98.14	59.46	26.37
w/o \mathcal{L}_{reg}	18.62	17.83	12.59	7.48	1.42

Effect of selective transfer. As shown in Tab. 3, we study the effect of the proposed *selective transfer*. LINVIDEO and *Manual* replace the layers with indices {2–8, 10–13, 15–16, 23, 25, 30} with linear attention, while *Heuristic* replaces {3–11, 13–16, 23, 27, 30}. In the table, *Manual* clearly outperforms *Heuristic*, indicating that our

training-based layer selection is more effective than heuristic rules. LINVIDEO further improves upon *Manual*, showing that the learnable score r in Eq. (8) enables a progressive and stable conversion from quadratic to linear attention that benefits training. We also ablate the coefficient λ of $\mathcal{L}_{con} + \mathcal{L}_{reg}$ in Eq. (14). Across metrics and λ values, the performance variation is about 1%, indicating that LINVIDEO is not sensitive to λ . Finally, removing \mathcal{L}_{reg} leads to a notable performance drop, confirming its role in improving training (*i.e.*, reducing fluctuation of r) and eliminating rounding-induced errors (*i.e.*, s.t. $|r - \lceil r \rceil| < 10^{-3}$ for each r). Visualization of its effect is also provided in Fig. 3.

Table 4. Ablation results of ADM. “w/ \mathcal{L}_{mse} ” and “w/ \mathcal{L}_{DMD} ” denotes employ these two objectives to replace our \mathcal{L}_{ADM} in Eq. (14), respectively. “w/ \hat{s}_t^\dagger ” represents we employ \mathcal{L}_{ADM} but train an additional model initialized from Wan 1.3B [44], which is to approximate the score function \hat{s}_t , at the same time. Following DMD [52], we employ 5× training iterations (*i.e.*, 15K) for the additional learned score approximator in both “w/ \mathcal{L}_{DMD} ” and “w/ \hat{s}_t^\dagger ”.

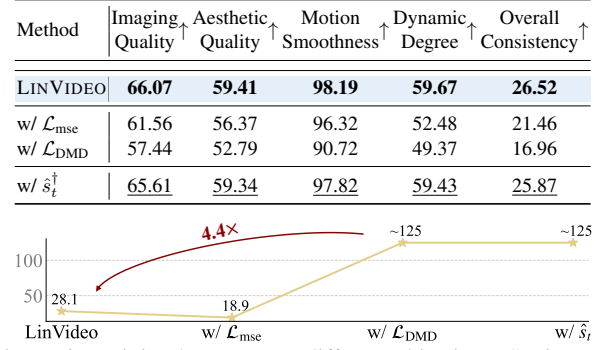


Figure 6. Training hours across different objectives. Settings are the same as those in Tab. 4.

Effect of ADM. We study several training objectives, as shown in Tab. 4. Our \mathcal{L}_{ADM} outperforms the naive \mathcal{L}_{mse} in Eq. (7) and the few-step distribution matching loss \mathcal{L}_{DMD} that aligns only p_g and p_0 (see Sec. 4.2), with a clear margin. In addition, \mathcal{L}_{ADM} reduces training time by $\sim 4.4\times$ compared with \mathcal{L}_{DMD} and the \hat{s}_t^\dagger variant, both of which require training an extra model to estimate \hat{s}_t . Besides, our LINVIDEO transfers the model smoothly and progressively from quadratic- to linear-attention *flow models*. Thus, it is reasonable to view u_θ as a *flow model* throughout this process. Experimentally, using u_θ itself to compute \hat{s}_t is more accurate, and thus achieves higher performance than \hat{s}_t^\dagger , which trains a separate score approximator.

6. Conclusion

In this work, we explore accelerating the video diffusion model (DM) inference with linear attention in a post-training, *data-free* manner. We first observe that replacing different quadratic attention layers with linear attention leads to large performance disparities. To address this, we propose *selective transfer*, which automatically and

progressively converts a target number of layers to linear attention while minimizing performance loss. Furthermore, finding that existing objectives are ineffective and inefficient in our scenarios, we introduce an *anytime distribution matching* (ADM) objective that aligns sample distributions with the original model across all timesteps in the sampling trajectory. This substantially improves output quality. Extensive experiments demonstrate that LINVIDEO delivers lossless acceleration across different benchmarks.

References

- [1] Yoshua Bengio, Nicholas Léonard, and Aaron Courville. Estimating or propagating gradients through stochastic neurons for conditional computation, 2013. 5
- [2] Boyuan Chen, Diego Martí Monso, Yilun Du, Max Simchowitz, Russ Tedrake, and Vincent Sitzmann. Diffusion forcing: Next-token prediction meets full-sequence diffusion. *arXiv preprint arXiv:2407.01392*, 2024. 2
- [3] Junsong Chen, Yuyang Zhao, Jincheng Yu, Ruihang Chu, Junyu Chen, Shuai Yang, Xianbang Wang, Yicheng Pan, Daquan Zhou, Huan Ling, Haozhe Liu, Hongwei Yi, Hao Zhang, Muyang Li, Yukang Chen, Han Cai, Sanja Fidler, Ping Luo, Song Han, and Enze Xie. Sana-video: Efficient video generation with block linear diffusion transformer, 2025. 1, 2
- [4] Karan Dalal, Daniel Koceja, Gashon Hussein, Jiarui Xu, Yue Zhao, Youjin Song, Shihao Han, Ka Chun Cheung, Jan Kautz, Carlos Guestrin, Tatsunori Hashimoto, Sanmi Koyejo, Yejin Choi, Yu Sun, and Xiaolong Wang. One-minute video generation with test-time training, 2025. 1, 2
- [5] Tri Dao. Flashattention-2: Faster attention with better parallelism and work partitioning, 2023. 6, 7
- [6] DeepSeek-AI, Aixin Liu, Bei Feng, Bing Xue, Bingxuan Wang, Bochao Wu, Chengda Lu, Chenggang Zhao, Chengqi Deng, Chenyu Zhang, Chong Ruan, Damai Dai, Daya Guo, Dejian Yang, Deli Chen, Dongjie Ji, Erhang Li, Fangyun Lin, Fucong Dai, Fuli Luo, Guangbo Hao, Guanting Chen, Guowei Li, H. Zhang, Han Bao, Hanwei Xu, Haocheng Wang, Haowei Zhang, Honghui Ding, Huajian Xin, Huazuo Gao, Hui Li, Hui Qu, J. L. Cai, Jian Liang, Jianzhong Guo, Jiaqi Ni, Jiashi Li, Jiawei Wang, Jin Chen, Jingchang Chen, Jingyang Yuan, Junjie Qiu, Junlong Li, Junxiao Song, Kai Dong, Kai Hu, Kaige Gao, Kang Guan, Kexin Huang, Kuai Yu, Lean Wang, Lecong Zhang, Lei Xu, Leyi Xia, Liang Zhao, Litong Wang, Liyue Zhang, Meng Li, Miaojun Wang, Mingchuan Zhang, Minghua Zhang, Minghui Tang, Mingming Li, Ning Tian, Panpan Huang, Peiyi Wang, Peng Zhang, Qiancheng Wang, Qihao Zhu, Qinyu Chen, Qiushi Du, R. J. Chen, R. L. Jin, Ruiqi Ge, Ruisong Zhang, Ruizhe Pan, Runji Wang, Runxin Xu, Ruoyu Zhang, Ruyi Chen, S. S. Li, Shanghai Lu, Shangyan Zhou, Shanhuan Chen, Shaoqing Wu, Shengfeng Ye, Shengfeng Ye, Shirong Ma, Shiyu Wang, Shuang Zhou, Shuiping Yu, Shunfeng Zhou, Shuteng Pan, T. Wang, Tao Yun, Tian Pei, Tianyu Sun, W. L. Xiao, Wangding Zeng, Wanjia Zhao, Wei An, Wen Liu, Wenfeng Liang, Wenjun Gao, Wenqin Yu, Wentao Zhang, X. Q. Li, Xiangyue Jin, Xianzu Wang, Xiao Bi, Xiaodong Liu, Xiaohan Wang, Xiaojin Shen, Xiaokang Chen, Xiaokang Zhang, Xiaosha Chen, Xiaotao Nie, Xiaowen Sun, Xiaoxiang Wang, Xin Cheng, Xin Liu, Xin Xie, Xingchao Liu, Xingkai Yu, Xinnan Song, Xinxia Shan, Xinyi Zhou, Xinyu Yang, Xinyuan Li, Xuecheng Su, Xuheng Lin, Y. K. Li, Y. Q. Wang, Y. X. Wei, Y. X. Zhu, Yang Zhang, Yanhong Xu, Yanhong Xu, Yanping Huang, Yao Li, Yao Zhao, Yaofeng Sun, Yaohui Li, Yaohui Wang, Yi Yu, Yi Zheng, Yichao Zhang, Yifan Shi, Yiliang Xiong, Ying He, Ying Tang, Yishi Piao, Yisong Wang, Yixuan Tan, Yiyang Ma, Yiyuan Liu, Yongqiang Guo, Yu Wu, Yuan Ou, Yuchen Zhu, Yuduan Wang, Yue Gong, Yuheng Zou, Yujia He, Yukun Zha, Yunfan Xiong, Yunxian Ma, Yuting Yan, Yuxiang Luo, Yuxiang You, Yuxuan Liu, Yuyang Zhou, Z. F. Wu, Z. Z. Ren, Ze-hui Ren, Zhangli Sha, Zhe Fu, Zhean Xu, Zhen Huang, Zhen Zhang, Zhenda Xie, Zhengyan Zhang, Zhewen Hao, Zhibin Gou, Zhicheng Ma, Zhigang Yan, Zhihong Shao, Zhipeng Xu, Zhiyu Wu, Zhongyu Zhang, Zhuoshu Li, Zihui Gu, Zijia Zhu, Zijun Liu, Zilin Li, Ziwei Xie, Ziyang Song, Ziyi Gao, and Zizheng Pan. Deepseek-v3 technical report, 2025. 1
- [7] Hangliang Ding, Dacheng Li, Runlong Su, Peiyuan Zhang, Zhijie Deng, Ion Stoica, and Hao Zhang. Efficient-vdit: Efficient video diffusion transformers with attention tile, 2025. 2
- [8] Steven K. Esser, Jeffrey L. McKinstry, Deepika Bablani, Rathinakumar Appuswamy, and Dharmendra S. Modha. Learned step size quantization, 2020. 2
- [9] Xin Gao, Li Hu, Siqi Hu, Mingyang Huang, Chaonan Ji, Dechao Meng, Jinwei Qi, Pengchong Qiao, Zhen Shen, Yafei Song, et al. Wan-s2v: Audio-driven cinematic video generation. *arXiv preprint arXiv:2508.18621*, 2025. 2
- [10] Yu Gao, Jiancheng Huang, Xiaopeng Sun, Zequn Jie, Yujie Zhong, and Lin Ma. Matten: Video generation with mamba-attention, 2024. 2
- [11] Xingtong Ge, Xin Zhang, Tongda Xu, Yi Zhang, Xinjie Zhang, Yan Wang, and Jun Zhang. Senseflow: Scaling distribution matching for flow-based text-to-image distillation, 2025. 5
- [12] Google DeepMind. Veo 3, 2025. Accessed: 2025-10-02. 2
- [13] Albert Gu and Tri Dao. Mamba: Linear-time sequence modeling with selective state spaces, 2024. 2
- [14] Jonathan Ho, Ajay Jain, and Pieter Abbeel. Denoising diffusion probabilistic models, 2020. 3
- [15] Jonathan Ho, Tim Salimans, Alexey Gritsenko, William Chan, Mohammad Norouzi, and David J. Fleet. Video diffusion models, 2022. 3
- [16] Jiancheng Huang, Gengwei Zhang, Zequn Jie, Siyu Jiao, Yinlong Qian, Ling Chen, Yunchao Wei, and Lin Ma. M4v: Multi-modal mamba for text-to-video generation, 2025. 2
- [17] Ziqi Huang, Yinan He, Jiashuo Yu, Fan Zhang, Chenyang Si, Yuming Jiang, Yuanhan Zhang, Tianxing Wu, Qingyang Jin, Nattapol Chanpaisit, et al. Vbench: Comprehensive benchmark suite for video generative models. In *Proceedings of the IEEE/CVF Conference on Computer Vision and Pattern Recognition*, pages 21807–21818, 2024. 4, 6, 12

[18] Angelos Katharopoulos, Apoorv Vyas, Nikolaos Pappas, and François Fleuret. Transformers are rnns: Fast autoregressive transformers with linear attention, 2020. 3

[19] Weijie Kong, Qi Tian, Zijian Zhang, Rox Min, Zuozhuo Dai, Jin Zhou, Jiangfeng Xiong, Xin Li, Bo Wu, Jianwei Zhang, Katrina Wu, Qin Lin, Junkun Yuan, Yanxin Long, Aladdin Wang, Andong Wang, Changlin Li, Duojun Huang, Fang Yang, Hao Tan, Hongmei Wang, Jacob Song, Jiawang Bai, Jianbing Wu, Jinbao Xue, Joey Wang, Kai Wang, Mengyang Liu, Pengyu Li, Shuai Li, Weiyang Wang, Wenqing Yu, Xincheng Deng, Yang Li, Yi Chen, Yutao Cui, Yuanbo Peng, Zhentao Yu, Zhiyu He, Zhiyong Xu, Zixiang Zhou, Zunnan Xu, Yangyu Tao, Qinglin Lu, Songtao Liu, Dax Zhou, Hongfa Wang, Yong Yang, Di Wang, Yuhong Liu, Jie Jiang, and Caesar Zhong. Hunyuandvideo: A systematic framework for large video generative models, 2025. 1, 2, 3

[20] Kuaishou. Kliing ai, 2024. Accessed: 2024-06-30. 1, 2

[21] Black Forest Labs. Flux, 2024. 1

[22] Xingyang Li, Muyang Li, Tianle Cai, Haocheng Xi, Shuo Yang, Yujun Lin, Lvmi Zhang, Songlin Yang, Jinbo Hu, Kelly Peng, Maneesh Agrawala, Ion Stoica, Kurt Keutzer, and Song Han. Radial attention: $o(n \log n)$ sparse attention with energy decay for long video generation, 2025. 1, 2, 7

[23] Yanjing Li, Sheng Xu, Xianbin Cao, Xiao Sun, and Baochang Zhang. Q-DM: An efficient low-bit quantized diffusion model. In *Thirty-seventh Conference on Neural Information Processing Systems*, 2023. 3

[24] Akide Liu, Zeyu Zhang, Zhixin Li, Xuehai Bai, Yizeng Han, Jiasheng Tang, Yuanjie Xing, Jichao Wu, Mingyang Yang, Weihua Chen, Jiahao He, Yuanyu He, Fan Wang, Gholamreza Haffari, and Bohan Zhuang. Fpsattention: Training-aware fp8 and sparsity co-design for fast video diffusion, 2025. 2

[25] Xingchao Liu, Chengyue Gong, and Qiang Liu. Flow straight and fast: Learning to generate and transfer data with rectified flow. In *ICLR*, 2022. 3

[26] Ilya Loshchilov and Frank Hutter. Decoupled weight decay regularization, 2019. 6

[27] Nanye Ma, Mark Goldstein, Michael S. Albergo, Nicholas M. Boffi, Eric Vanden-Eijnden, and Saining Xie. Sit: Exploring flow and diffusion-based generative models with scalable interpolant transformers, 2024. 6, 12

[28] Markus Nagel, Rana Ali Amjad, Mart van Baalen, Christos Louizos, and Tijmen Blankevoort. Up or down? adaptive rounding for post-training quantization, 2020. 5

[29] Kepan Nan, Rui Xie, Penghao Zhou, Tiehan Fan, Zhenheng Yang, Zhijie Chen, Xiang Li, Jian Yang, and Ying Tai. Openvid-1m: A large-scale high-quality dataset for text-to-video generation. *arXiv preprint arXiv:2407.02371*, 2024. 12, 13

[30] OpenAI. Video generation models as world simulators, 2024. Accessed: 2025-04-09. 1, 2, 3

[31] William Peebles and Saining Xie. Scalable diffusion models with transformers. In *Proceedings of the IEEE/CVF international conference on computer vision*, pages 4195–4205, 2023. 1, 2

[32] Weiming Ren, Huan Yang, Ge Zhang, Cong Wei, Xinrun Du, Wenhao Huang, and Wenhui Chen. Consisti2v: Enhancing visual consistency for image-to-video generation, 2024. 6

[33] Tim Salimans and Jonathan Ho. Progressive distillation for fast sampling of diffusion models. In *ICLR*, 2022. 3

[34] Team Seawead, Ceyuan Yang, Zhijie Lin, Yang Zhao, Shanchuan Lin, Zhibei Ma, Haoyuan Guo, Hao Chen, Lu Qi, Sen Wang, et al. Seaweed-7b: Cost-effective training of video generation foundation model. *arXiv preprint arXiv:2504.08685*, 2025. 2

[35] Noam Shazeer, Azalia Mirhoseini, Krzysztof Maziarz, Andy Davis, Quoc Le, Geoffrey Hinton, and Jeff Dean. Outrageously large neural networks: The sparsely-gated mixture-of-experts layer, 2017. 2

[36] Jiaming Song, Chenlin Meng, and Stefano Ermon. Denoising diffusion implicit models. *ArXiv*, abs/2010.02502, 2021. 3

[37] Yang Song, Jascha Sohl-Dickstein, Diederik P. Kingma, Abhishek Kumar, Stefano Ermon, and Ben Poole. Score-based generative modeling through stochastic differential equations. In *ICLR*, 2021. 2, 5, 6

[38] Wenhao Sun, Rong-Cheng Tu, Yifu Ding, Zhao Jin, Jingyi Liao, Shunyu Liu, and Dacheng Tao. Vorta: Efficient video diffusion via routing sparse attention, 2025. 2

[39] Xin Tan, Yuetao Chen, Yimin Jiang, Xing Chen, Kun Yan, Nan Duan, Yibo Zhu, Dixin Jiang, and Hong Xu. Dsv: Exploiting dynamic sparsity to accelerate large-scale video dit training, 2025. 2

[40] Hugo Touvron, Thibaut Lavril, Gautier Izacard, Xavier Martinet, Marie-Anne Lachaux, Timothée Lacroix, Baptiste Rozière, Naman Goyal, Eric Hambro, Faisal Azhar, Aurelien Rodriguez, Armand Joulin, Edouard Grave, and Guillaume Lample. Llama: Open and efficient foundation language models, 2023. 1

[41] Ashish Vaswani, Noam Shazeer, Niki Parmar, Jakob Uszkoreit, Llion Jones, Aidan N. Gomez, Łukasz Kaiser, and Illia Polosukhin. Attention is all you need, 2023. 3

[42] Fu-Yun Wang, Ling Yang, Zhaoyang Huang, Mengdi Wang, and Hongsheng Li. Rectified diffusion: Straightness is not your need in rectified flow. *arXiv preprint arXiv:2410.07303*, 2024. 3

[43] Hongjie Wang, Chih-Yao Ma, Yen-Cheng Liu, Ji Hou, Tao Xu, Jialiang Wang, Felix Juefei-Xu, Yaqiao Luo, Peizhao Zhang, Tingbo Hou, Peter Vajda, Niraj K. Jha, and Xiaoliang Dai. Lingen: Towards high-resolution minute-length text-to-video generation with linear computational complexity, 2025. 1, 2

[44] WanTeam, :, Ang Wang, Baole Ai, Bin Wen, Chaojie Mao, Chen-Wei Xie, Di Chen, Feiwei Yu, Haiming Zhao, Jianxiao Yang, Jianyuan Zeng, Jiayu Wang, Jingfeng Zhang, Jingen Zhou, Jinkai Wang, Jixuan Chen, Kai Zhu, Kang Zhao, Keyu Yan, Lianghua Huang, Mengyang Feng, Ningyi Zhang, Pandeng Li, Pingyu Wu, Ruihang Chu, Ruili Feng, Shiwei Zhang, Siyang Sun, Tao Fang, Tianxing Wang, Tianyi Gui, Tingyu Weng, Tong Shen, Wei Lin, Wei Wang, Wei Wang, Wenmeng Zhou, Wente Wang, Wenting Shen, Wenyuan Yu, Xianzhong Shi, Xiaoming Huang, Xin Xu, Yan Kou, Yangyu

Lv, Yifei Li, Yijing Liu, Yiming Wang, Yingya Zhang, Yitong Huang, Yong Li, You Wu, Yu Liu, Yulin Pan, Yun Zheng, Yuntao Hong, Yupeng Shi, Yutong Feng, Zeyinzi Jiang, Zhen Han, Zhi-Fan Wu, and Ziyu Liu. Wan: Open and advanced large-scale video generative models, 2025. 1, 2, 3, 4, 6, 7, 8, 12, 13, 14, 15

[45] Haocheng Xi, Shuo Yang, Yilong Zhao, Chenfeng Xu, Muyang Li, Xiuyu Li, Yujun Lin, Han Cai, Jintao Zhang, Dacheng Li, Jianfei Chen, Ion Stoica, Kurt Keutzer, and Song Han. Sparse videogen: Accelerating video diffusion transformers with spatial-temporal sparsity, 2025. 1, 2, 6, 7

[46] Enze Xie, Junsong Chen, Junyu Chen, Han Cai, Haotian Tang, Yujun Lin, Zhekai Zhang, Muyang Li, Ligeng Zhu, Yao Lu, and Song Han. Sana: Efficient high-resolution image synthesis with linear diffusion transformers. *arXiv preprint arXiv:2410.10629*, 2024. 2

[47] Enze Xie, Junsong Chen, Junyu Chen, Han Cai, Haotian Tang, Yujun Lin, Zhekai Zhang, Muyang Li, Ligeng Zhu, Yao Lu, and Song Han. SANA: Efficient high-resolution text-to-image synthesis with linear diffusion transformers. In *The Thirteenth International Conference on Learning Representations*, 2025. 1

[48] Ruyi Xu, Guangxuan Xiao, Haofeng Huang, Junxian Guo, and Song Han. Xattention: Block sparse attention with anti-diagonal scoring, 2025. 2, 6

[49] Shuo Yang, Haocheng Xi, Yilong Zhao, Muyang Li, Jintao Zhang, Han Cai, Yujun Lin, Xiuyu Li, Chenfeng Xu, Kelly Peng, Jianfei Chen, Song Han, Kurt Keutzer, and Ion Stoica. Sparse videogen2: Accelerate video generation with sparse attention via semantic-aware permutation, 2025. 6

[50] Zhuoyi Yang, Jiayan Teng, Wendi Zheng, Ming Ding, Shiyu Huang, Jiazheng Xu, Yuanming Yang, Wenqi Hong, Xiaohan Zhang, Guanyu Feng, Da Yin, Yuxuan Zhang, Weihan Wang, Yean Cheng, Bin Xu, Xiaotao Gu, Yuxiao Dong, and Jie Tang. Cogvideox: Text-to-video diffusion models with an expert transformer, 2025. 1, 2, 3

[51] Tianwei Yin, Michaël Gharbi, Taesung Park, Richard Zhang, Eli Shechtman, Frédéric Durand, and William T. Freeman. Improved distribution matching distillation for fast image synthesis. In *NeurIPS*, 2024. 2, 5, 6, 7, 13, 14, 15

[52] Tianwei Yin, Michaël Gharbi, Richard Zhang, Eli Shechtman, Frédéric Durand, William T. Freeman, and Taesung Park. One-step diffusion with distribution matching distillation. In *CVPR*, pages 6613–6623, 2024. 2, 5, 8

[53] Tianwei Yin, Qiang Zhang, Richard Zhang, William T Freeman, Frédéric Durand, Eli Shechtman, and Xun Huang. From slow bidirectional to fast causal video generators. *arXiv preprint arXiv:2412.07772*, 2024. 5

[54] Tianwei Yin, Qiang Zhang, Richard Zhang, William T Freeman, Frédéric Durand, Eli Shechtman, and Xun Huang. From slow bidirectional to fast autoregressive video diffusion models. In *CVPR*, 2025. 5

[55] Zhihang Yuan, Hanling Zhang, Pu Lu, Xuefei Ning, Linfeng Zhang, Tianchen Zhao, Shengen Yan, Guohao Dai, and Yu Wang. Difastattn: Attention compression for diffusion transformer models, 2024. 6

[56] Jintao Zhang, Haoxu Wang, Kai Jiang, Shuo Yang, Kaiwen Zheng, Haocheng Xi, Ziteng Wang, Hongzhou Zhu, Min Zhao, Ion Stoica, Joseph E. Gonzalez, Jun Zhu, and Jianfei Chen. Sla: Beyond sparsity in diffusion transformers via fine-tunable sparse-linear attention, 2025. 2, 7

[57] Jintao Zhang, Chendong Xiang, Haofeng Huang, Jia Wei, Haocheng Xi, Jun Zhu, and Jianfei Chen. Spargeattention: Accurate and training-free sparse attention accelerating any model inference, 2025. 2

[58] Michael Zhang, Kush Bhatia, Hermann Kumbong, and Christopher Re. The hedgehog & the porcupine: Expressive linear attentions with softmax mimicry. In *The Twelfth International Conference on Learning Representations*, 2024. 1, 3

[59] Peiyuan Zhang, Yongqi Chen, Haofeng Huang, Will Lin, Zhengzhong Liu, Ion Stoica, Eric Xing, and Hao Zhang. Vsa: Faster video diffusion with trainable sparse attention, 2025. 2, 7

[60] Peiyuan Zhang, Yongqi Chen, Runlong Su, Hangliang Ding, Ion Stoica, Zhengzhong Liu, and Hao Zhang. Fast video generation with sliding tile attention, 2025. 1, 2

[61] Yuechen Zhang, Jinbo Xing, Bin Xia, Shaoteng Liu, Bo-hao Peng, Xin Tao, Pengfei Wan, Eric Lo, and Jiaya Jia. Training-free efficient video generation via dynamic token carving, 2025. 2

[62] Tianchen Zhao, Tongcheng Fang, Haofeng Huang, Rui Wan, Widyadewi Soedarmadji, Enshu Liu, Shiyao Li, Zinan Lin, Guohao Dai, Shengen Yan, Huazhong Yang, Xuefei Ning, and Yu Wang. Vudit-q: Efficient and accurate quantization of diffusion transformers for image and video generation. In *The Thirteenth International Conference on Learning Representations*, 2025. 6

[63] Tianchen Zhao, Ke Hong, Xinhao Yang, Xuefeng Xiao, Huixia Li, Feng Ling, Ruiqi Xie, Siqi Chen, Hongyu Zhu, Yichong Zhang, and Yu Wang. Paroattention: Pattern-aware reordering for efficient sparse and quantized attention in visual generation models, 2025. 2

[64] Yanli Zhao, Andrew Gu, Rohan Varma, Liang Luo, Chien-Chin Huang, Min Xu, Less Wright, Hamid Shojanazeri, Myle Ott, Sam Shleifer, Alban Desmaison, Can Balioglu, Pritam Damania, Bernard Nguyen, Geeta Chauhan, Yuchen Hao, Ajit Mathews, and Shen Li. Pytorch fsdp: Experiences on scaling fully sharded data parallel, 2023. 12

[65] Dian Zheng, Ziqi Huang, Hongbo Liu, Kai Zou, Yinan He, Fan Zhang, Yuanhan Zhang, Jingwen He, Wei-Shi Zheng, Yu Qiao, and Ziwei Liu. Vbench-2.0: Advancing video generation benchmark suite for intrinsic faithfulness, 2025. 6, 7, 12

[66] Zangwei Zheng, Xiangyu Peng, Tianji Yang, Chenhui Shen, Shenggui Li, Hongxin Liu, Yukun Zhou, Tianyi Li, and Yang You. Open-sora: Democratizing efficient video production for all. *arXiv preprint arXiv:2412.20404*, 2024. 3

Appendix

This document supplements the main paper as follows:

- Sec. A provides more implementation details;
- Sec. B details the effect of hyperparameter α of Eq. (10);
- Sec. C provides additional ablation studies for α ;
- Sec. D gives the derivation of score difference (*i.e.*, Eq. (13));
- Sec. E presents examples of temporal jitter incurred by naive objective (*i.e.*, Eq. (7));
- Sec. F shows the results of directly distilling the original DM into a 4-step model with linear attention;
- Sec. G provides detailed setups for heuristic search in Tab. 3;
- Sec. H presents visualization examples of our LINVIDEO.

A. More Implementation Details

In this section, we provide additional implementation details. Before training, we first collect inputs and outputs from Wan [44] across different sampling steps using prompts from OpenVid [29]. Each input/output contains 81 frames (21 frames in latent space), with an original resolution of 480p for Wan 1.3B and 720p for Wan 14B. During training, we use Pytorch FSDP [64] with a warm-up phase covering $\frac{1}{10}$ of the total training epochs, and set the global batch size to 48 for Wan 1.3B and 64 for Wan 14B. The learning rate follows a cosine annealing schedule, starting from 1×10^{-4} . For other hyperparameters, we set $\lambda = 0.01$, and α follows a linear decay from 20 to 2. For evaluation, we sample 5 videos for each unaugmented text prompt across the 8 dimensions in VBench [17]. For VBench-2.0 [65], we generate 3 videos per augmented text prompt across all dimensions, except for the Diversity dimension, where we generate 20 videos for each prompt.

B. Effect of α

As mentioned in the main text, we annealing decay the parameter α from large to small. This encourages r to move more adaptively at the initial phase to improve the training loss, but forces it to 0.0/1.0 in the later phase. To understand this behavior, we provide a visualization in Fig. I. As shown in this figure, when α is large, the function remains nearly constant (close to 1.0) from $r^{(l)} = 0.5$ extending towards both boundaries, resulting in near-zero gradients in most regions. This flat landscape allows r to explore more freely during initial training. Conversely, when α is small, the gradient remains significant across a broader range, effectively pushing r towards the boundaries (0.0 or 1.0) in later training stages.

C. Ablation for α

Here, we provide additional ablation studies for α of \mathcal{L}_{reg} . As demonstrated in Tab. I, when we narrow or expand the

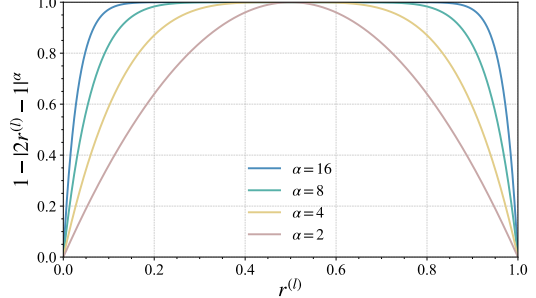


Figure I. Effect of α on $1 - |2r^{(l)} - 1|^\alpha$ of Eq. (10).

range of α , the variation in all metrics stays within 0.03, which shows that our loss is not sensitive to changes in the chosen α values. In addition, this range of α yields strong final performance for models from 1.3B to 14B (Tab. 1), demonstrating good generalization. We also verify experimentally that using a dynamically changing α gives non-negligible improvements compared with using a fixed α , which confirms the benefit of our design: α encourages free exploration in the early stage of training and is gradually guided toward 0.0/1.0 only in the later stage.

Table I. Ablation results of α . Our LINVIDEO employs $20 \rightarrow 2$ as the range of α .

Range of α	Imaging Quality \uparrow	Aesthetic Quality \uparrow	Motion Smoothness \uparrow	Dynamic Degree \uparrow	Overall Consistency \uparrow
$20 \rightarrow 2$	66.07	59.41	98.19	59.67	26.57
$16 \rightarrow 4$	66.09	59.38	98.16	59.70	26.54
$24 \rightarrow 1$	66.06	59.40	98.20	59.65	26.56
$4 \rightarrow 4$	65.87	59.08	98.10	59.08	26.27

D. Derivation of Eq. (13)

In this section, we provide a derivation of Eq. (13). Following Ma *et al.* [27] (their Eq. (9)), the score s_t associated with $\hat{\mathbf{x}}_t$ and estimated by \mathbf{u}_θ can be written as

$$s_t(\hat{\mathbf{x}}_t) = \sigma_t^{-1} \frac{\alpha_t \mathbf{u}_\theta(\hat{\mathbf{x}}_t) - \dot{\alpha}_t \hat{\mathbf{x}}_t}{\dot{\alpha}_t \sigma_t - \alpha_t \dot{\sigma}_t}, \quad (\text{I})$$

where α_t, σ_t are the noise schedules and $\dot{\alpha}_t, \dot{\sigma}_t$ are their first-order derivatives with respect to t . For the *rectified flow models* [44] considered in this work, we take $\alpha_t = 1 - t$ and $\sigma_t = t$. Substituting these schedules into the above expression yields

$$s_t(\hat{\mathbf{x}}_t) = \frac{1}{t} \frac{(1-t)\mathbf{u}_\theta(\hat{\mathbf{x}}_t) + \hat{\mathbf{x}}_t}{-t - (1-t)} = -\frac{1}{t} ((1-t)\mathbf{u}_\theta(\hat{\mathbf{x}}_t) + \hat{\mathbf{x}}_t). \quad (\text{II})$$

Likewise, the score \hat{s}_t estimated by $\hat{\mathbf{u}}_\theta$ corresponding to $\hat{\mathbf{x}}_t$ is given by

$$\hat{s}_t(\hat{\mathbf{x}}_t) = -\frac{1}{t} ((1-t)\hat{\mathbf{u}}_\theta(\hat{\mathbf{x}}_t) + \hat{\mathbf{x}}_t). \quad (\text{III})$$

Therefore, the score difference is

$$s_t(\hat{\mathbf{x}}_t) - \hat{s}_t(\hat{\mathbf{x}}_t) = -\frac{1-t}{t} (\mathbf{u}_\theta(\hat{\mathbf{x}}_t) - \hat{\mathbf{u}}_\theta(\hat{\mathbf{x}}_t)). \quad (\text{IV})$$

E. Temporal Jitter of Naive Objective

We provide examples in Fig. II using the naive training objective \mathcal{L}_{mse} (*i.e.*, Eq. (7)), where the results clearly exhibit temporal jitter.



Figure II. A segment of 6 adjacent frames from an 81-frame, 480p, 16 fps video generated by the linear-attention Wan 1.3B [44] trained with the naive objective. Other settings are the same as those for LINVIDEO. Both the dog’s legs (*Upper*) and the butterflies (*Lower*) exhibit severe temporal jitter.

F. Directly combine Few-step Distillation with Linear Attention

As shown in Tab. II, we observe that directly combining a few-step distillation with linear attention replacement (*i.e.*, our *selective transfer*) leads to severe performance degradation. This motivates a two-stage pipeline, *viz.*, LINVIDEO→DMD2 [51]. In the first stage, linear attention is introduced and already attains strong performance; in the second stage, few-step distillation is applied to further accelerate the model. This two-stage design stabilizes training and avoids the collapse observed with the direct combination.

G. Details of Heuristic Search

For the *Heuristic* search method in the ablation study, we use 128 prompts from OpenVid [29]. Starting from the original DM, at each step we consider all remaining quadratic attention layers, construct modified variants where only one candidate layer is replaced by a linear attention layer, and measure the resulting output differences. We then permanently replace the layer that yields the smallest

Table II. Performance for the few-step distilled linear attention Wan 1.3B [44]. “LINVIDEO + DMD2” denotes that we first employ LINVIDEO to obtain a linear attention DM and then use DMD2 [51] to distill it to the 4-step version. “ST + DMD2” implies that we combine our *selective transfer* and DMD2 to obtain the 4-step linear attention model in a single training stage.

Method	Imaging Quality ↑	Aesthetic Quality ↑	Motion Smoothness ↑	Dynamic Degree ↑	Overall Consistency ↑
LINVIDEO + DMD2	65.62	57.74	97.32	61.26	25.94
ST + DMD2	48.72	39.64	73.85	41.97	11.06

difference and repeat this procedure based on the updated model until the desired number of target layers has been selected.

H. Visualization Results

In this section, we present randomly selected samples generated by LINVIDEO without any cherry-picking, as shown in Figs. III–IV. For a more detailed inspection, we recommend zooming in to closely examine the individual frames.

Prompt: “A volcano erupts in the distance, glowing lava rivers flowing against a darkened sky.”



Prompt: “A pod of dolphins leaps out of the sparkling ocean in graceful arcs, splashing back into the water as the horizon glows with sunset; the camera follows from the side, keeping a continuous rhythm with their motion.”



Prompt: “A massive elephant walks slowly across a sunlit savannah, dust rising around its feet, the warm glow of sunset illuminating the horizon; the camera moves steadily forward alongside, emphasizing the grandeur of its stride.”

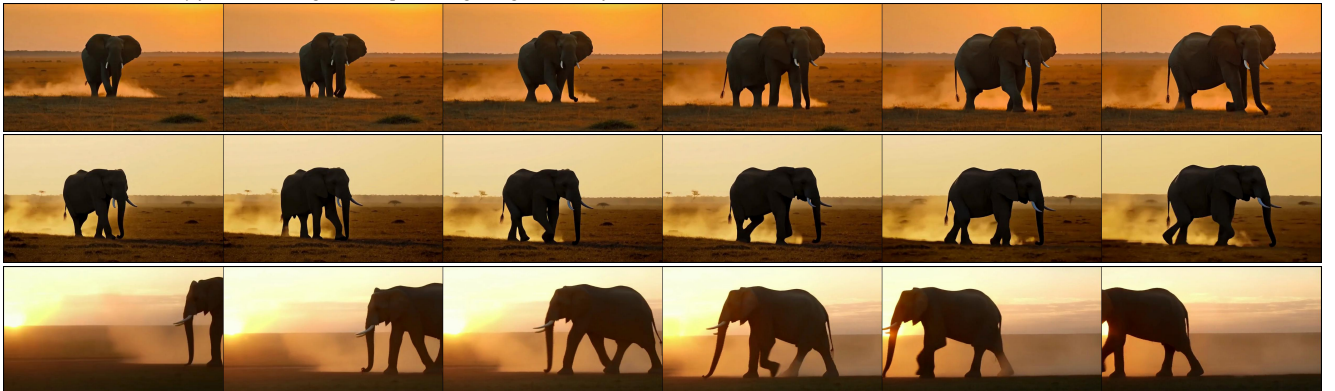


Figure III. Visual results at 480p across Wan 1.3B [44] (Upper), 1.3B LINVIDEO (Middle), and 1.3B LINVIDEO+ 4-step DMD2 [51] (Lower).

Prompt: “Retro 80s Monster Horror Comedy Movie Scene: Color film, children’s bedroom bathed in soft, warm light. Plush monsters of various sizes and colors are having a chaotic party, jumping on the bed, dancing to upbeat music, and throwing confetti. The walls are adorned with posters of classic 80s movies, and the room is filled with the playful laughter of children.”



Prompt: “A drone camera circles around a beautiful historic church built on a rocky outcropping along the Amalfi Coast, the view showcases historic and magnificent architectural details and tiered pathways and patios, waves are seen crashing against the rocks below as the view overlooks the horizon of the coastal waters and hilly landscapes of the Amalfi Coast Italy, several distant people are seen walking and enjoying vistas on patios of the dramatic ocean views, the warm glow of the afternoon sun creates a magical and romantic feeling to the scene, the view is stunning captured with beautiful photography.”



Prompt: “An extreme close-up of an gray-haired man with a beard in his 60s, he is deep in thought pondering the history of the universe as he sits at a cafe in Paris, his eyes focus on people offscreen as they walk as he sits mostly motionless, he is dressed in a wool coat suit coat with a button-down shirt, he wears a brown beret and glasses and has a very professorial appearance, and the end he offers a subtle closed-mouth smile as if he found the answer to the mystery of life, the lighting is very cinematic with the golden light and the Parisian streets and city in the background, depth of field, cinematic 35mm film.”



Figure IV. Visual results at 720p across Wan 14B [44] (Upper), 14B LINVIDEO (Middle), and 14B LINVIDEO+ 4-step DMD2 [51] (Lower).